Downregulation of HAS-2 regulates the chondrocyte cytoskeleton and induces cartilage degeneration by activating the RhoA/ROCK signaling pathway

JUNLONG YANG[1], LIU WANG[2], ZHONGJIE ZHANG[1], QING SUN[3] and YUAN ZHANG[4]

[1]Department of Pain, The Affiliated Hospital of Guizhou Medical University, Guiyang, Guizhou 550004; [2]Department of Pain, Affiliated Hospital of North Sichuan Medical College, Nanchong, Sichuan 637002; [3]Department of Pain, Guizhou Provincial People's Hospital, Guiyang, Guizhou 550002; [4]Department of Orthopedic Surgery, First Affiliated Hospital of Kunming Medical University, Kunming, Yunnan 650032, P.R. China

Received November 4, 2022; Accepted April 18, 2023

DOI: 10.3892/ijmm.2023.5260

Abstract. Osteoarthritis (OA) is a progressive joint disorder, which is principally characterized by the degeneration and destruction of articular cartilage. The cytoskeleton is a vital structure that maintains the morphology and function of chondrocytes, and its destruction is a crucial risk factor leading to chondrocyte degeneration and OA. Hyaluronan synthase-2 (HAS-2) is a key enzyme in synthesizing hyaluronic acid (HA) *in vivo*. The synthesis of high molecular weight HA catalyzed by HAS-2 serves a vital role in joint movement and homeostasis; however, it is unclear what important role HAS-2 plays in maintaining chondrocyte cytoskeleton morphology and in cartilage degeneration. The present study downregulated the expression of HAS-2 by employing 4-methylumbelliferone (4-MU) and RNA interference. *In vitro* experiments, including reverse transcription-quantitative PCR, western blotting, laser scanning confocal microscopy and flow cytometry were subsequently performed. The results revealed that downregulation of HAS-2 could activate the RhoA/ROCK signaling pathway, cause morphological abnormalities, decrease expression of the chondrocyte cytoskeleton proteins and promote chondrocyte apoptosis. *In vivo* experiments, including immunohistochemistry and Mankin's scoring, were performed to verify the effect of HAS-2 on the chondrocyte cytoskeleton, and it was revealed that inhibition of HAS-2 could cause cartilage degeneration. In conclusion, the present results revealed that downregulation of HAS-2 could activate the RhoA/ROCK pathway, cause abnormal morphology and decrease chondrocyte cytoskeleton protein expression, leading to changes in the signal transduction and biomechanical properties of chondrocytes, promotion of chondrocyte apoptosis and the induction of cartilage degeneration. Moreover, the clinical application of 4-MU may cause cartilage degeneration. Therefore, targeting HAS-2 may provide a novel therapeutic strategy for delaying chondrocyte degeneration, and the early prevention and treatment of OA.

Correspondence to: Dr Yuan Zhang, Department of Orthopedic Surgery, First Affiliated Hospital of Kunming Medical University, 295 Xichang Road, Kunming, Yunnan 650032, P.R. China
E-mail: zhhyya@163.com

Key words: hyaluronan synthase-2, 4-methylumbelliferone, chondrocyte cytoskeleton, osteoarthritis

Introduction

Osteoarthritis (OA) is the most common degenerative joint disease, which is characterized by cartilage damage, synovial inflammation, joint capsule thickening and joint pain (1). To date, the treatment for OA has primarily focused on the alleviation of pain and inflammation using nonsteroidal anti-inflammatory drugs or other agents; however, these drugs cannot delay the progression of OA (2,3). Therefore, new therapeutic strategies are urgently needed, which could delay the progression of OA.

Chondrocytes are a single cellular component of the mature articular cartilage and serve a key role in its degeneration. The cytoskeleton is composed of microfilaments, microtubules and intermediate fibers, which are themselves composed of actin, tubulin and vimentin, respectively. Notably, the cytoskeleton is an important structure for maintaining the morphology and function of chondrocytes (4,5). Changes in the cytoskeleton can affect the signal transduction and mechanical properties of chondrocytes, which can lead to OA (6,7). Furthermore, destruction of the chondrocyte cytoskeleton has been reported to be a key risk factor leading to chondrocyte degeneration and OA (8). Therefore, the chondrocyte cytoskeleton is the target of novel therapy research; in particular, how to effectively protect the chondrocyte cytoskeleton is the focus of the current treatment research. The RhoA/ROCK signaling pathway, which is mainly composed of RhoA protein and ROCK, is important in signal transduction and participates in important physiological functions, such as cytoskeleton reorganization, cell cycle and apoptosis regulation (9).

Hyaluronan synthase (HAS) is the key enzyme of hyaluronic acid (HA) synthesis *in vivo*; therefore, the expression

of HAS directly affects the synthesis of endogenous HA. There are three types of HAS isozymes: HAS-1, HAS-2 and HAS-3 (10). Different HAS isozymes serve different roles in the synthesis of endogenous HA. HAS-2 has the highest catalytic activity and expression in all stages of embryonic development. High molecular weight HA synthesized by HAS isozymes has an important role in joint movement and the maintenance of intra-articular homeostasis (11,12). The HA receptor CD44 on the surface of chondrocytes can interact with various cytoskeleton proteins, and is related to the intracellular RhoA/ROCK signaling pathway and a variety of cellular metabolic processes (13,14). However, as a key enzyme in the synthesis of HA *in vivo*, it remains to be determined what important role HAS-2 plays in maintaining normal chondrocyte cytoskeleton morphology and in cartilage degeneration.

4-Methylumbelliferone (4-MU) is an approved drug for treating biliary spasms, and it is also a highly effective and low-toxic specific HAS inhibitor, which can reduce the synthesis of HA by inhibiting HAS (15). However, HA is also an important component of the extracellular matrix at the site of chronic inflammation in a variety of diseases, including type I diabetes, multiple sclerosis and various malignant tumors (16). It has previously been reported that when using 4-MU, the synthesis of HA in the extracellular matrix of tumor tissues, such as mouse pancreatic ductal adenocarcinoma, melanoma and hepatocellular carcinoma, is decreased, inhibiting tumor invasion and metastasis and thus resulting in an antitumor effect (17,18). However, to the best of our knowledge, whether the clinical application of 4-MU will lead to cartilage degeneration by inhibiting chondrocyte HAS-2 has not been studied.

The present study aimed to determine whether HAS-2 is a key molecule regulating the chondrocyte cytoskeleton. In the present study, HAS-2 was downregulated by 4-MU treatment and HAS-2-short hairpin RNA (shRNA) transduction. The changes in the chondrocyte cytoskeleton were detected *in vitro*, and the possible mechanism underlying the abnormal chondrocyte cytoskeleton induced by the downregulation of HAS-2 was assessed. In addition, the degeneration of articular cartilage was evaluated following intra-articular injection of 4-MU in rats, and the injury effect of clinical application of 4-MU on articular cartilage was clarified. The present results indicated that targeting HAS2 may be used to develop new strategies for delaying chondrocyte degeneration and for the early prevention of OA.

Materials and methods

Cell culture and animal grouping. The C28/I2 immortalized human chondrocyte line (Haling Biotechnology Co., Ltd.) was cultured in DMEM/F-12 (Hyclone; Cytiva) containing 10% fetal bovine serum (Hyclone; Cytiva) and 1% penicillin-streptomycin (Beijing Solarbio Science & Technology Co., Ltd.) at 37˚C in a humidified atmosphere containing 5% CO_2. Cells were harvested by trypsinization and fresh culture medium was added to generate single-cell suspensions for use in the subsequent experiments. The culture medium was replaced with fresh medium every 48 h and the cells were passaged every 2-3 days.

A total of 20 male Sprague-Dawley rats (age, 8 weeks; weight, 180-220 g) were obtained from the Animal Center of Kunming Medical University (Kunming, China). The rats were housed at a constant temperature (25˚C) at 55% humidity under a 12-h light/dark cycle with *ad libitum* access to water and standard chow. Rats were divided into the following four groups (n=5 rats/group): Control (normal saline), 1% DMSO, 1.0 mM 4-MU and 2.0 mM 4-MU. 4-MU (cat. no. M1381; MilliporeSigma) was dissolved in DMSO (cat. no. D2650; MilliporeSigma) as a cosolvent and filtered using a 0.22-μm sterile filter unit. The rats were anesthetized by intraperitoneal injection of pentobarbital (35 mg/kg). According to the grouping, 100 μl saline, DMSO or 4-MU was injected into the left knee joint cavity of the rats using a 1-ml syringe under aseptic conditions. The rats were injected once every 3 days for a total of five times. On day 15, all of the rats were sacrificed by cervical dislocation under anesthesia through an intraperitoneal injection of pentobarbital sodium (50 mg/kg), and respiratory arrest was used to confirm animal death. Subsequently, the left knee joint was collected and stored in 4% paraformaldehyde for 24 h at 4˚C. All animal experiments were performed in accordance with the approval of the Institutional Committee on the Care and Use of Animals of Kunming Medical University (approval no. Kmmu20220992).

MTT assay. The MTT Cell Proliferation and Cytotoxicity Assay Kit (cat. no. C0009; Beyotime Institute of Biotechnology) was used to determine the proliferation curve of C28/I2 cells and to assess the cytotoxic effects of 4-MU on C28/I2 cells, according to the manufacturer's protocol. C28/I2 cells ($5x10^3$ cells/well) were plated in seven 96-well plates in triplicate and cultured in growth medium. The seven microplates were incubated for 24, 48, 72, 96, 120, 144 and 168 h, respectively. Subsequently, 10 μl MTT solution was added to each well and the cells were incubated at 37˚C for 4 h. Formazan solution (100 μl) was then added to each well and incubated at 37˚C for a further 4 h until all of the purple crystals were dissolved. The optical density was measured at 570 nm using a microplate reader (SpectraMax 190; Molecular Devices, LLC). In addition, cells were plated in 96-well plates in triplicate and cultured in growth medium for 48 h. The adherent cells were then divided into eight groups and treated with different concentrations of 4-MU (0, 0.25, 0.50, 0.75 and 1.00 mM) or DMSO (0, 0.125, 0.25, 0.375 and 0.5%) for another 48 h at 37˚C. The cytotoxic effects of different concentrations of 4-MU and DMSO were determined using the aforementioned method.

Plasmid construction and transduction. The shRNA targeting the HAS-2 gene was designed using the Sigma shRNA design program (MilliporeSigma) and synthesized by Generay Biotech Co., Ltd. The HAS-2-shRNA target sequence was 5'-CGAAGCGATTATCACTGGATT-3' and a scramble sequence (5'-TTCGAAGAGGTTATCACTCAG-3') was used as a negative control (HAS-2-scramble). C28/I2 cells in the logarithmic growth phase were seeded in 6-well plates at a concentration of $1x10^5$ cells/well, and were cultured under saturated humidity at 37˚C and 5% CO_2 in DMEM/F-12 containing 10% fetal bovine serum. When the cell density reached >80%, serum-free OPTI-MEM (Gibco; Thermo Fisher Scientific, Inc.) was used for the culture. pLKO.1-puro lentiviral vectors

were used to silence HAS-2. pLKO.1-shRNA-puro constructs were generated using a 2nd generation lentiviral system by inserting the shRNA sequences into a pLKO.1-puro vector (MiaoLing Plasmid Sharing Platform). Lentiviruses were generated by transfecting 293T cells (China Center for Type Culture Collection) with pLKO.1-shRNA (8 μg), packaging (psPAX2, 6 μg) and envelope (pMD2G, 2 μg) plasmids using Lipofectamine® 2000 (Invitrogen; Thermo Fisher Scientific, Inc.). Lentiviral particles were harvested 48 h post-transfection and were added to C28/I2 cells at a multiplicity of infection of 60. To create stable cell lines, 24 h post-transduction, C28/I2 cells were selected using 2 μg/ml puromycin (MilliporeSigma) for 24 h and were maintained in 1 μg/ml puromycin. At 48 h post-transduction, the interference efficiency of HAS-2-shRNA was determined using reverse transcription-quantitative PCR (RT-qPCR). All subsequent experiments were performed 48 h post-transduction.

Western blotting. C28/I2 cells were cultured for 48 h and were then treated with culture medium containing 4-MU (0, 0.25, 0.50, 0.75 or 1.00 mM) or 0.5% DMSO. After 48 h at 37˚C, images of the C28/I2 cells were captured under a light inverted microscope and total protein was subsequently isolated from C28/I2 cells. Briefly, cells were lysed in RIPA buffer containing a protease inhibitor cocktail (Beijing Solarbio Science & Technology Co., Ltd.). The concentration of the protein samples was determined using the BCA Protein Assay Kit (cat. no. P0010; Beyotime Institute of Biotechnology). Equal volumes of protein samples (50 μg/lane) were separated by SDS-PAGE on 10% gels and electroblotted onto a polyvinylidene fluoride membrane (MilliporeSigma) using standard procedures. Membranes were blocked for 1 h at room temperature with 5% non-fat milk in Tris-buffered saline plus 0.5% Tween-20. The transferred blots were then incubated sequentially with rabbit anti-HAS2 antibody (1:1,000; cat. no. ab9485) and rabbit anti-GAPDH antibody (1:2,500; cat. no. ab199794) (both from Abcam) overnight at 4˚C. To examine the effect of HAS-2-shRNA on the RhoA/ROCK signaling pathway, C28/I2 cells were transduced with HAS-2-shRNA for 48 h. Subsequently, the target protein blots were incubated with primary antibodies against: RhoA (1:1,000; cat. no. 10749-1-AP), ROCK1 (1:1,000; cat. no. 21850-1-AP) and ROCK2 (1:1,000; cat. no. 21645-1-AP) (all from Wuhan Sanying Biotechnology) overnight at 4˚C. Subsequently, the membranes were incubated with HRP-conjugated goat anti-rabbit secondary antibody (1:2,000; cat. no. ab6721; Abcam) for 1 h at room temperature. Protein bands were visualized using an enhanced chemiluminescence detection kit (Tiangen Biotech Co., Lt.) and recorded on radiographic film (Bio-Rad Laboratories, Inc.). Semi-quantitative analysis of protein band intensity was conducted using ImageJ V1.8.0 software (National Institutes of Health) and normalized to the internal loading control, GAPDH.

Immunofluorescence and semi-quantitative analysis. C28/I2 cell suspensions were plated in a confocal glass petri dish (diameter, 15 mm) in triplicate at ~5x10^4 cells (1 ml) per well and cultured in growth medium for 48 h. The medium was then replaced and the cells were cultured with medium containing different concentrations (0, 0.5, and 1.0 mM) of 4-MU, or 0.5% DMSO for another 48 h at 37˚C in a humidified atmosphere containing 5% CO_2. Subsequently, the cells were fixed with 4% formaldehyde for 15 min at 37˚C, permeabilized with 0.1% Triton X-100 in PBS for 10 min at room temperature, and blocked with 3% BSA (MilliporeSigma) and 0.05% Tween 20 in PBS for 30 min at room temperature. For transduced cells, after 48 h of transduction, cells were fixed as aforementioned and underwent immunofluorescence staining. F-actin was stained using the CytoPainter Phalloidin-iFluor 555 Reagent kit (1:1,000; cat. no. ab176756; Abcam) overnight at 4˚C and the nuclei were stained with DAPI (Beijing Solarbio Science & Technology Co., Ltd.) for 5 min at room temperature. Vimentin was stained with anti-vimentin antibody (1:130; cat. no. ab92547; Abcam) overnight at 4˚C and goat anti-rabbit IgG H&L (Alexa Fluor® 488) (1:130; cat. no. ab150077; Abcam) for 1 h at room temperature in the dark, and the nuclei were stained with DAPI for 5 min at room temperature. Tubulin was stained with anti-β tubulin antibody (1:400; cat. no. ab179513; Abcam) overnight at 4˚C and goat anti-rabbit IgG H&L (Alexa Fluor 488) (1:200) for 1 h at room temperature in the dark, and the nuclei were stained with PI (1:20; cat. no. ab14083; Abcam) for 5 min at room temperature. Fluorescence images were acquired and semi-quantitative analysis was performed using the Leica TCS SP5 laser scanning confocal microscope (LSCM; Leica Microsystems GmbH) using the LAS AF Lite 2.3.6 Software (Leica Microsystems GmbH).

To perform statistical analysis of vimentin, actin and tubulin staining, and to assess the variation in these cytoskeleton components following treatment with 4-MU, the LSCM was adjusted to the appropriate parameters. All of the parameters were fixed to capture the confocal image under the condition of a x20 objective lens. The fluorescence intensity of the cytoskeleton components was measured using the LAS AF Lite2.3.6 software. The fluorescence determination method is performed by operating the mouse to outline a single cell, and the software automatically calculates the fluorescence value of the cytoskeleton protein under the corresponding fluorescence channel in the delineated area. The fluorescence intensity of a certain cytoskeleton protein in a single chondrocyte can be calculated according to this method. A total of 20 chondrocytes for each cytoskeletal protein in each group were measured and analyzed. In addition, the subcellular structure images were collected under a x100 objective lens, and the morphology of the chondrocyte cytoskeleton proteins was observed.

Relative quantification of mRNA using RT-qPCR. After C28/I2 cells were transduced for 48 h, total RNA was extracted using the RNeasy kit (Qiagen GmbH) according to the manufacturer's protocol. Total RNA concentration was determined by measuring the absorbance at 260/280 nm using a spectrophotometer (BioTeke Corporation). Total RNA (1 μg) was then reverse-transcribed using the High-Capacity cDNA RT kit (Thermo Fisher Scientific, Inc.) according to the manufacturer's protocol. qPCR was performed using an ABI Prism 7900 sequence detection system and 2X T5 Fast qPCR Mix (SYBR Green I) reagents (TsingKe Biological Technology). GAPDH was utilized as a housekeeping gene for normalizing mRNA expression levels. Each qPCR reaction contained 10 μl 2X T5 Fast qPCR Mix, 0.8 μl primers (10 μM; Table I), 0.4 μl 50X ROX Reference Dye I, 1 μl

Table I. Primer sequences used in reverse transcription-quantitative PCR.

Gene	Forward primer, 5'-3'	Reverse primer, 5'-3'
HAS-2	CAGATGGCTAAACCAGCAGACC	GAATCCAGTGATAATCGCTTCGTAG
RhoA	CAGGTAGAGTTGGCTTTGTGG	TCTGCCTTCTTCAGGTTTCA
ROCKI	TAACCTCCCAGAGTCAAGAATT	TTTTGCTGCTTACCACAACATAC
ROCKII	CTTTATCATTTCCCAACCAAC	CCACTTCTGCTGCTCTTCTG
GAPDH	AACGGATTTGGTCGTATTGGG	CCTGGAAGATGGTGATGGGAT

HAS-2, hyaluronan synthase-2.

DNA template (20 ng/μl), and PCR-grade water to obtain a final volume of 20 μl. The thermal cycler conditions were as follows: Hold for 10 min at 95˚C, followed by 40 cycles of a two-step PCR consisting of a 95˚C step for 10 sec and a 60˚C step for 30 sec. For each sample, qPCR reactions were performed in triplicate, and the average Cq was calculated. The Cq values of the different samples were compared using the $2^{-\Delta\Delta Cq}$ method (19).

Cell apoptosis assays. Cell apoptosis was measured using the Annexin V-FITC apoptosis detection kit (Beyotime Institute of Biotechnology) and a flow cytometer (CyFlow Space; Sysmex Partec GmbH). Following infection of C28/I2 cells with lentivirus-containing supernatant for 48 h, apoptosis was detected. According to the manufacturer's instructions, cells were incubated with 200 μl Annexin V-FITC and 10 μl PI in the dark at 25˚C for 10 min. The stained cells were analyzed using flow cytometry. All of the treatments were performed in triplicate. Cells positive for both PI and Annexin V-FITC were considered late apoptotic cells, and those negative for both Annexin V-FITC and PI were considered live cells. PI-positive and Annexin V-FITC-negative cells were considered necrotic cells, whereas PI-negative and Annexin V-FITC-positive cells were considered early apoptotic cells.

Histological evaluation. The rat knee joint samples were decalcified in 10% EDTA (pH 7.5). The decalcified specimens were trimmed, dehydrated and embedded in paraffin. Sections (6 μm) were cut in the sagittal plane, and were then deparaffinized with xylene and dehydrated with ethanol. Heat-induced antigen retrieval was performed with sodium citrate at 95˚C for 30 min. Endogenous peroxidase activity was blocked with 3% H_2O_2 for 20 min at room temperature and the treated sections were blocked for 1 h at room temperature with 10% goat serum (Beijing Solarbio Science & Technology Co., Ltd.). Subsequently, the sections were incubated with rabbit anti-F-actin antibody (1:200; cat. no. bs-1571R; Biosharp Life Sciences), anti-vimentin antibody (1:130; cat. no. ab92547; Abcam) or anti-β tubulin antibody (1:400; cat. no. ab179513; Abcam) overnight at 4˚C. HRP-conjugated goat anti-rabbit secondary antibody (1:1,000; cat. no. ab6721; Abcam) was then added and incubated at 37˚C for 30 min. Antigens were detected using the DAB kit (Beyotime Institute of Biotechnology) after 20 min of incubation at room temperature. Photomicrographs were captured under a light microscope (BX53; Olympus Corporation).

Hematoxylin and eosin (H&E) staining. Tissue samples were dewaxed by soaking the sections in xylene twice for 10 min, rinsing with distilled water for 30 sec, then soaking consecutively in 100, 100, 90, 80 and 70% alcohol for 5 min, and finally rinsing with tap water for 5 min three times. The samples were stained with hematoxylin (Beijing Solarbio Science & Technology Co., Ltd.) for 5 min at room temperature and rinsed with running water. Samples were then differentiated with 5% acetic acid for 1 min, washed with running water for 10 min, stained with eosin (Beijing Solarbio Science & Technology Co., Ltd.) for 1 min at room temperature, and rinsed three times with running water, for 5 min. The slices were dehydrated by placing them in 70, 80, 90 and 100% alcohol and xylene for 1 min each, and were then sealed with neutral glue, and covered with a coverslip. The tissues were examined using a light microscope (BX53; Olympus Corporation).

Safranin O/fast green staining. The dewaxing procedure was performed according to the H&E staining protocol, as aforementioned. The sections were then stained with hematoxylin for 5 min and rinsed with tap water for 10 min. The sections were dyed with 0.5% Fast Green FCF Stain Solution (Beijing Solarbio Science & Technology Co., Ltd.) for 3 min and then washed with tap water for 5 min three times. The sections were placed in 1% acetic acid for 5 sec, immersed in 1% safranin staining solution (Beijing Solarbio Science & Technology Co., Ltd.) for 2 min at room temperature, and then rinsed three times with distilled water for 5 min. Finally, the samples were dehydrated and sealed as aforementioned for H&E staining. The samples were examined using a light microscope (BX53; Olympus Corporation).

Cartilage severity in the tibial plateau was evaluated according to modified Mankin's histologic grading system, and a cartilage destruction score was assigned for each knee sample by three independent assessors. The Mankin's score assesses structure, cellularity, matrix staining and tidemark integrity. For matrix staining, safranin O staining was used. The Mankin's score ranges from 0 points for healthy cartilage to 14 points for the most severe cartilage lesions (20). The final score for each sample was based on the most severe histological changes observed in multiple sections from each specimen. The Mankin's score was again divided into three stages depending on the score: Grade I (normal cartilage, 0-1 points), grade II (mild to moderate degenerative change, 2-9 points), and grade III (severe degenerative change, ≥10 points). A total of five rats were assessed in each group, giving a total of 20 rats for all tests.

Statistical analysis. All data were analyzed using SPSS Statistics 23.0 software (IBM Corp.). Data are presented as the mean ± SD unless stated otherwise. Graphs were drawn using GraphPad Prism software (version 8.0). ImageJ (1.8.0; National Institutes of Health) software was used for immunohistochemistry, immunofluorescence and western blot analyses. For *in vitro* studies, the lowest number of replicates per experiment was three. All data were tested for normality of distribution using the Shapiro-Wilk test. One-way analysis of variance with Tukey's post hoc test was used to compare the parametric data between groups. For Mankin's score data, the Kruskal-Wallis test with Dunn's post hoc test was used. $P<0.05$ was considered to indicate a statistically significant difference.

Results

Determination of logarithmic growth phase. The proliferation curve of C28/I2 cells was detected by MTT assay (Fig. 1A). The cells were in the growth incubation period and proliferated slowly 1-2 days after inoculation. The cells then proliferated rapidly in the logarithmic growth phase from day 3 to 5, before entering the plateau period on days 6-7. The whole proliferation curve is in the shape of an 'S'. In the present study, all cell experiments were performed in the logarithmic growth phase after 2 days of subculture.

Effect of 4-MU and DMSO on C28/I2 cell viability. The MTT assay was performed to assess the cytotoxic effects of 4-MU and DMSO on C28/I2 cells. The C28/I2 cells were treated with various concentrations of 4-MU (0, 0.25, 0.50, 0.75 and 1.00 mM) or DMSO (0, 0.125, 0.25, 0.375 and 0.5%) for 48 h. After 48 h, cell cytotoxicity was tested using the MTT assay; no significant cytotoxicity was observed regardless of the experimental concentrations (Fig. 1B). Therefore, the present study adopted 4-MU at a concentration of <1.0 mM and DMSO at a concentration of <0.5% in the subsequent cell experiments.

4-MU inhibits the expression of HAS-2. Western blot analysis was performed to investigate the effect of 4-MU on the protein expression levels of HAS-2. After C28/I2 cells were treated with 4-MU for 48 h, the total proteins were extracted from each group. As shown in Fig. 1C and D, the protein expression levels of HAS-2 were significantly decreased in cells in the 4-MU groups compared with those in the control group in a concentration-dependent manner. Since 4-MU is insoluble in water, DMSO was used as a co-solvent in the present study. Therefore, it is necessary to test whether the experimental concentration of DMSO affects the expression of HAS-2 when 4-MU is used. However, there was no significant difference in the expression levels of HAS-2 in the DMSO group. Therefore, 4-MU was defined as an inhibitor of HAS-2 in the subsequent experiments.

Effect of 4-MU on C28/I2 cell morphology. The morphological changes of C28/I2 cells were detected under an inverted microscope. C28/I2 cells were treated with various concentrations of 4-MU (0, 0.25, 0.5, 0.75 and 1.0 mM) for 48 h. The cells in the control and 0.5% DMSO groups were uniform in size and small in shape, mainly small triangles and polygons, and the intercellular background was clean and free of impurities (Fig. 1Ea and b). 4-MU was able to induce cell morphological changes in a concentration-dependent manner. As shown in Fig. 1Ec-f, the morphology and size of the cells were different, the cytoplasmic volume decreased, the pseudopodia increased and became slender, and the intercellular connections decreased; when cells were treated with 0.75 mM 4-MU, the pseudopodia began to appear discontinuous or broken, the background impurities increased and the cell adhesion ability decreased. Thus, these results suggested that 4-MU could change the morphology of chondrocytes in a dose-dependent manner and this was not associated with DMSO.

4-MU regulates the distribution and expression of the chondrocyte cytoskeleton proteins. To better observe the fine structure of cytoskeleton proteins, a LSCM was used to assess the morphology of cytoskeleton proteins in individual cells. Fig. 2 shows representative images of immunofluorescence staining of C28/I2 cells treated with 4-MU for 48 h.

As shown in Fig. 2A, vimentin was filamentous in the control and 0.5% DMSO groups, forming an intertwined reticular structure that runs through the cytoplasm, and it was denser near the cell membrane. The arrangement of vimentin was disordered following treatment with 0.5 mM 4-MU; the polarity disappeared and the distribution decreased. In the 1.0 mM 4-MU treatment group, the distribution of vimentin was sparse and loose, and only local dense distribution could be seen around the nucleus. The tubulin in the control and 0.5% DMSO groups appeared to be in a radial pattern, was uniformly distributed from the nucleus to the cell membrane and dense radial aggregation sites could be seen near the nucleus. Notably, the distribution of tubulin was sparse and its density decreased in response to 0.5 mM 4-MU, whereas in the 1.0 mM 4-MU treatment group, the distribution of tubulin concentrated around the nucleus and was markedly decreased near the cell membrane, and microtubule breakage could be seen. The actin in the control and 0.5% DMSO groups showed filamentous distribution around the cytoplasm near the cell membrane and less around the nucleus; in addition, most of the actin appeared as thick long stress filaments, arranged along the longitudinal axis of the cells and a few actin fibers were arranged in a reticular cross pattern. After 4-MU treatment, the thick and long actin stress filaments disappeared and the fine actin fibers were arranged in a sparse, disorganized network.

The present study semi-quantitatively measured the fluorescence intensity of the cytoskeleton proteins, thus providing a visual and clear indication of the content of these proteins. As shown in Fig. 2B, the expression of vimentin was high in the control and 0.5% DMSO groups. In the 4-MU groups, the expression of vimentin significantly decreased in a concentration-dependent manner compared with that in the control group. The expression of tubulin was similar to that of vimentin, it also decreased in a concentration-dependent manner in response to 4-MU. However, the expression of actin was slightly decreased in the 4-MU treatment groups compared with that in the control group, but this was not significant. These data indicated that 4-MU regulates the distribution and expression of chondrocyte cytoskeleton proteins by inhibiting HAS-2, and thus affects the morphology of C28/I2 cells.

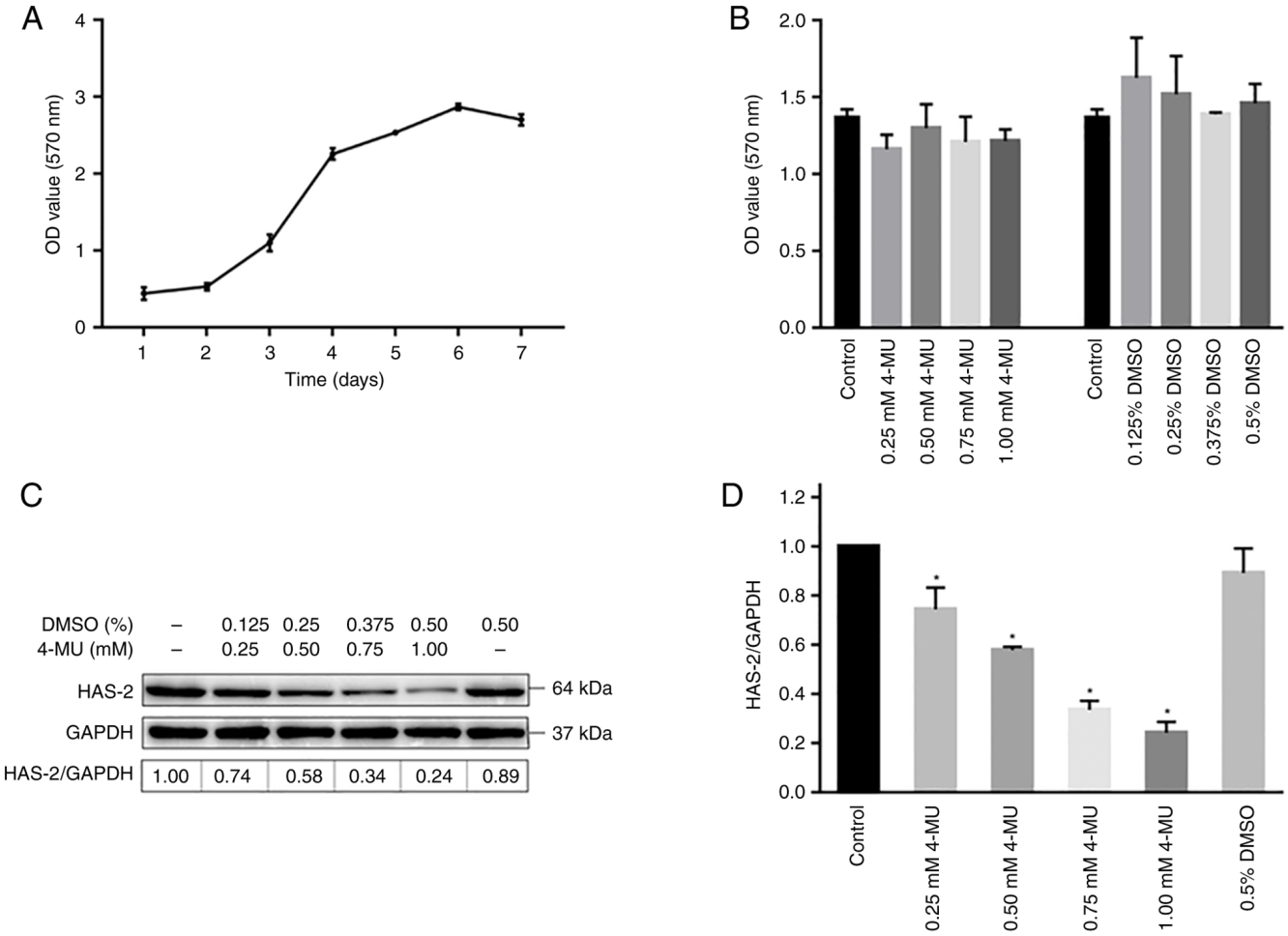

Figure 1. 4-MU leads to abnormal morphology of chondrocytes by inhibiting HAS-2. (A) Proliferation curve of C28/I2 cells was detected by MTT assay. (B) Cytotoxicity of various concentrations of 4-MU and DMSO on chondrocytes was determined at 48 h using the MTT assay. (C) C28/I2 cells were treated with 4-MU for 48 h and the protein expression levels of HAS-2 were assessed by western blotting. (D) HAS-2 expression was densitometrically semi-quantified and normalized to the levels of GAPDH. (E) Effects of different concentrations of 4-MU on the morphology of C28/I2 cells: (a) Control (0 mM 4-MU), (b) NC (0.5% DMSO), (c) 0.25, (d) 0.50, (e) 0.75 and (f) 1.00 mM 4-MU. Data are presented as the mean ± SD of three independent experiments. *P<0.05 vs. control group. 4-MU, 4-methylumbelliferone; HAS-2, hyaluronan synthase-2.

HAS-2-shRNA regulates the chondrocyte cytoskeleton. To eliminate the multiple effects of compound inhibitors, gene silencing was used to detect the effects of HAS-2-shRNA on the chondrocyte cytoskeleton. The gene silencing efficiency of HAS-2-shRNA was verified by RT-qPCR (Fig. S1). Subsequently, the chondrocyte cytoskeleton was observed

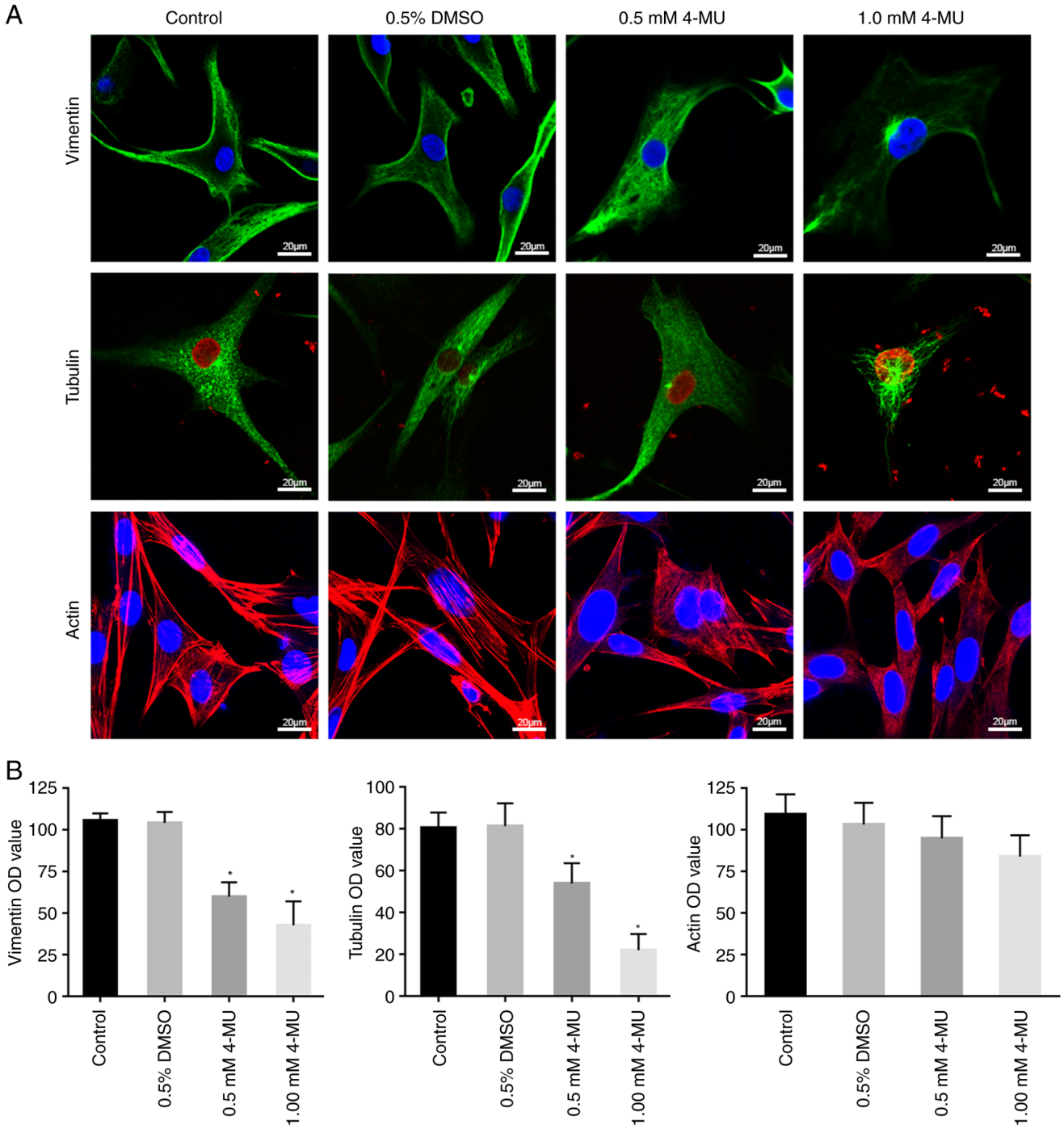

Figure 2. 4-MU regulates the distribution and expression of chondrocyte cytoskeleton proteins. (A) C28/I2 cells were treated with 4-MU for 48 h, and the distribution and expression of cytoskeleton proteins (vimentin, tubulin and actin) was observed by laser scanning confocal microscopy. Scale bars, 20 μm. (B) Fluorescence intensity of cytoskeleton proteins (vimentin, tubulin and actin) was semi-quantitatively analyzed. Data are presented as the mean ± SD. *P<0.05 vs. control group, n=20 chondrocytes/group. 4-MU, 4-methylumbelliferone.

using a LSCM. As shown in Fig. 3, similar to the results of 4-MU treatment, the expression levels of vimentin, tubulin and actin were decreased after HAS-2-shRNA transduction. However, there was no marked difference in the expression of cytoskeleton proteins between the HAS-2-scramble and control groups. Therefore, this verifies the regulatory role of HAS-2 on the chondrocyte cytoskeleton at the genetic level.

HAS-2-shRNA activates the RhoA/ROCK signaling pathway and promotes chondrocyte apoptosis. It has been reported that changes in the chondrocyte cytoskeleton are closely related to the RhoA/ROCK signaling pathway (21). However, to the best of our knowledge, the mechanism of HAS-2 in the regulation of the chondrocyte cytoskeleton is not yet known. Therefore, the present study detected changes in the RhoA/ROCK signaling pathway after HAS-2 gene silencing; it was observed that RhoA, ROCK1 and ROCK2 expression levels were significantly increased at the gene and protein levels (Fig. 4A-D). In addition, the effect of HAS-2-shRNA on chondrocyte apoptosis was assessed by flow cytometry. The

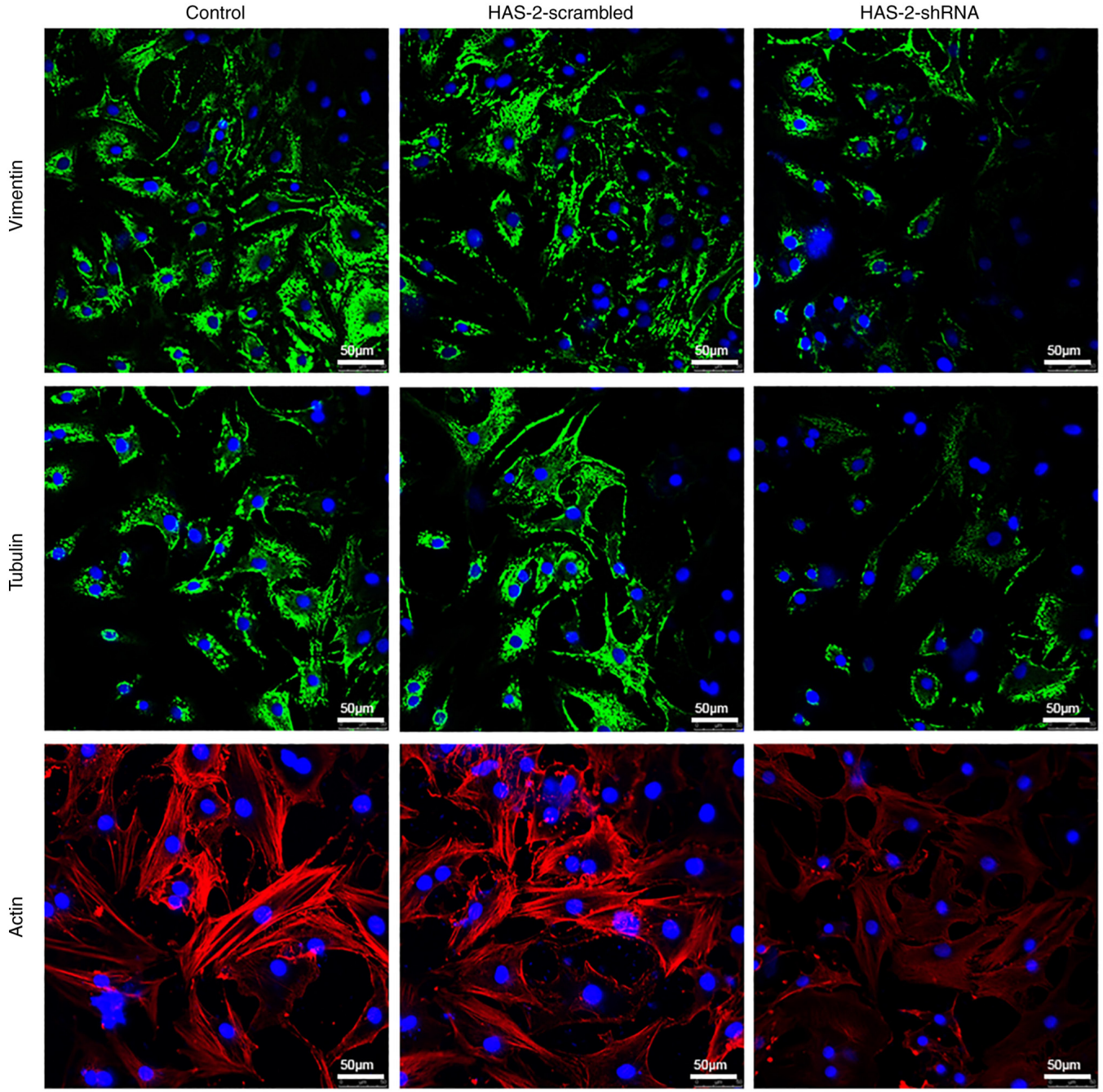

Figure 3. HAS-2-shRNA regulates the chondrocyte cytoskeleton. C28/I2 cells were transduced with HAS-2-shRNA, and the distribution and expression of cytoskeleton proteins (vimentin, tubulin and actin) was observed by laser scanning confocal microscopy. Scale bars, 50 μm. HAS-2, hyaluronan synthase-2; shRNA, short hairpin RNA.

results suggested that HAS-2-shRNA was able to promote the apoptosis of chondrocytes (Fig. 4E and F). These results suggested that downregulation of HAS-2 may activate the RhoA/ROCK signaling pathway, thus participating in regulation of the cytoskeleton and promoting chondrocyte apoptosis.

Immunohistochemical staining of cytoskeleton proteins in cartilage tissue. Immunohistochemistry was performed to detect the cytoskeleton proteins in rat articular cartilage samples. The cytoplasm of positive cells showed deep brown-yellow staining and the results are shown in Fig. 5. In vimentin staining, the chondrocytes in the control and 1% DMSO groups showed deep brown-yellow staining throughout the cartilage layer. In the cartilage layer of the 1.0 mM 4-MU group, compared with in the control group, the number of positive cells in the superficial layer and the middle layer was not markedly different, but the number of positive cells in the deep layer of cartilage was notably reduced. In the 2.0 mM 4-MU group, positive cells were only seen in the superficial layer of cartilage, but no positive cells were found in the middle and deep layers. In tubulin staining, positive brown-yellow-stained cells were seen in the cartilage layer of each group. Although the chondrocytes

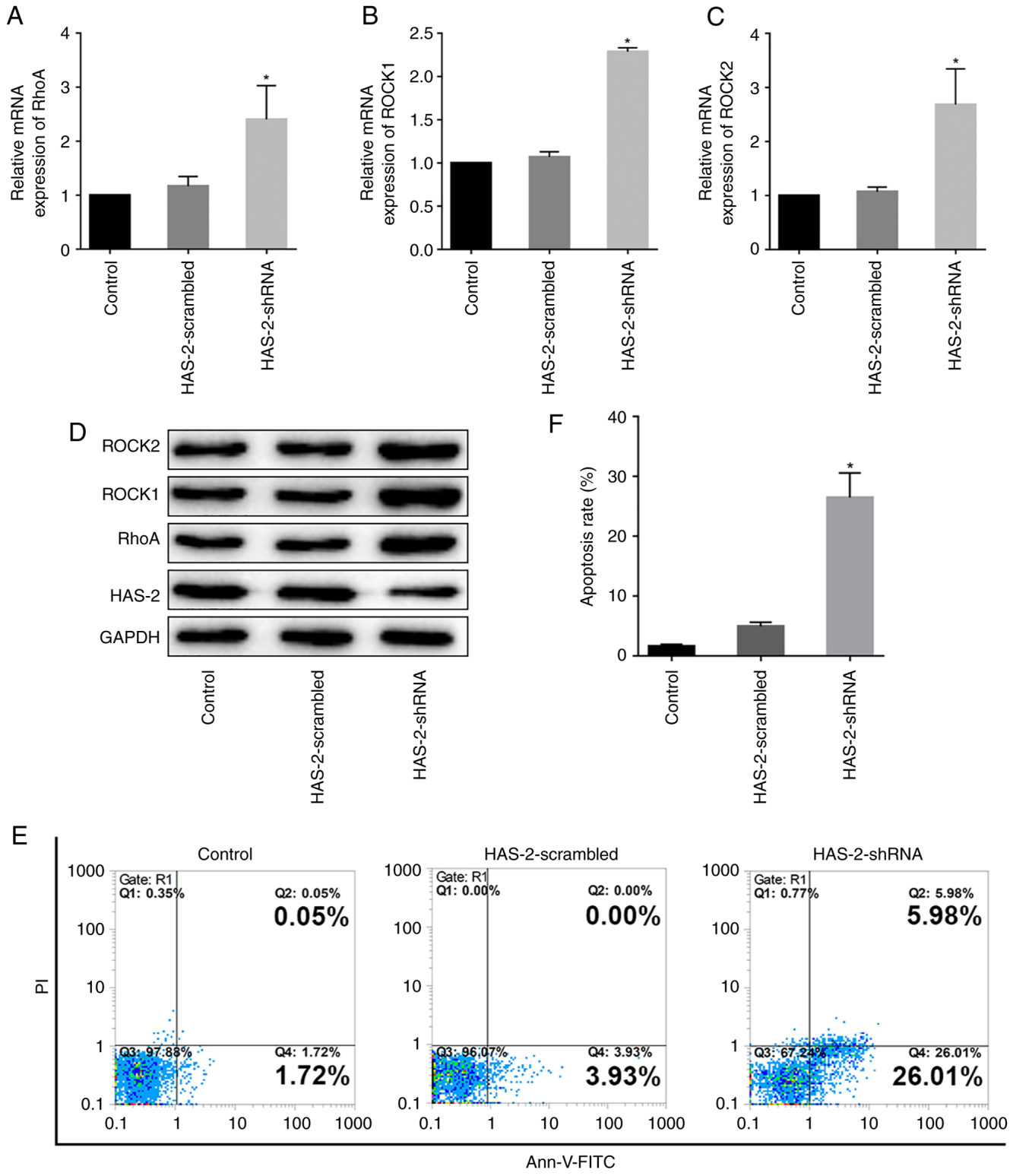

Figure 4. HAS-2-shRNA activates the RhoA/ROCK signaling pathway and promotes chondrocyte apoptosis. C28/I2 cells were transduced with HAS-2-shRNA or HAS-2-scrambled. The cells were harvested after 48 h, and the mRNA expression levels of (A) RhoA, (B) ROCK1 and (C) ROCK2, and (D) their protein expression levels were evaluated using reverse transcription-quantitative PCR and western blotting, respectively. (E) Flow cytometric analysis of Annexin V-FITC/PI staining was performed to determine the percentages of cells in early and late apoptosis. (F) Results are displayed in a histogram. Data are presented as the mean ± SD from three independent experiments. *P<0.05 vs. control group. HAS-2, hyaluronan synthase-2; shRNA, short hairpin RNA.

in the 4-MU group were disorderly arranged, there was no notable difference in the number of positive cells compared with that in the control group. In actin staining, the chondrocytes in the control and 1% DMSO groups showed deep brown-yellow staining throughout the cartilage layer. In the cartilage layer of the 1.0 and 2.0 mM 4-MU groups, the number of positive cells was markedly decreased, but the number of positive cells was similar between the two

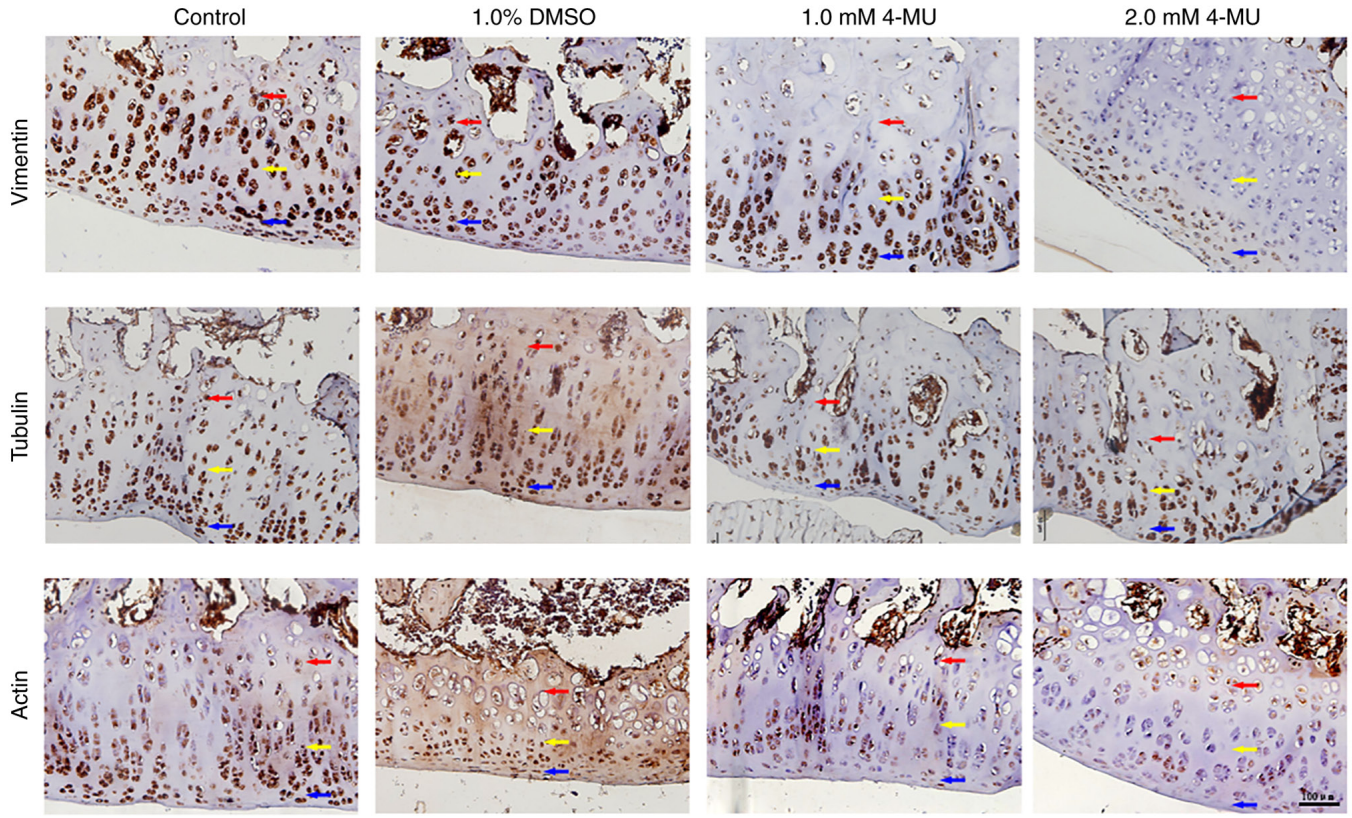

Figure 5. Immunohistochemical staining of cytoskeleton proteins in the cartilage tissue of rats after 4-MU treatment. After 4-MU was injected into the knee joint of rats, the expression of cytoskeleton proteins (vimentin, tubulin and actin) in the cartilage layer was observed by immunohistochemical staining. Red, yellow and blue arrows represent the deep layer, the middle layer and the superficial layer of cartilage areas, respectively. Scale bars: 100 μm. 4-MU, 4-methylumbelliferone.

groups. Taken together, these results suggested that 4-MU may also change the distribution and expression of the cytoskeleton in cartilage *in vivo*.

4-MU-induced inhibition of HAS-2 leads to cartilage degeneration in vivo. To investigate the effects of 4-MU-induced inhibition of HAS-2 expression on the progression of articular cartilage degeneration *in vivo*, histological analysis of cartilage was measured by H&E and safranin O staining, and cartilage degeneration was evaluated by Mankin's score. As shown in Fig. 6A, in the control and 1% DMSO groups, the articular cartilage was smooth and flat, the chondrocytes were arranged neatly, and the tidemark was regular. The safranin O staining results were similar in the two groups; enhanced staining was found in the articular surface and near the subchondral bone area in the cartilage layer. In the H&E staining images of the 1.0 mM 4-MU group, the articular cartilage surface was not smooth, the cartilage layer was slightly thinner, the arrangement of chondrocytes was irregular and the tidemark was complete. Notably, in the 2.0 mM 4-MU group, there was severe fibrosis on the surface of articular cartilage, chondrocytes were atrophied, exhibited a clustered distribution and disordered arrangement, the tidemark was still complete and cartilage tissue injury was more serious. In the safranin O staining images, the two 4-MU groups exhibited substantial loss of safranin O staining (indicative of aggrecan proteoglycan loss) occurring in the cartilage layer, and there was no marked difference in the staining between the two 4-MU groups.

According to the results of H&E and safranin O staining, the knee cartilage of rats was scored using the modified Mankin's histologic grading system (Fig. 6B). The scores in the control and 1% DMSO groups were low, thus indicating that there was no significant degeneration of cartilage tissue. Following injection with 4-MU, the degree of cartilage degeneration was significantly increased in a concentration-dependent manner. The Mankin's scores were significantly increased in the 4-MU groups compared with those in the control group. The degree of cartilage degeneration in the 4-MU groups appears to have reached the level of early and intermediate OA.

Discussion

OA, the most prevalent musculoskeletal disorder worldwide, is more frequent in older age groups and is developing into an increasingly important public health concern (22-24). Treatment of OA is limited to drugs, such as HA, corticosteroids and opioids (25,26). For example, intra-articular injection of HA has a wide range of applications in relieving OA pain and improving joint function; however, these drugs only temporarily ease swelling and chronic pain. In addition, these drugs can lead to deleterious side effects (23). Furthermore, repeated intra-articular injection brings pain and risk to patients. In the end-stage of OA, artificial joint replacement is the only choice for OA therapy (27). Therefore, it is necessary to identify a safe and effective therapeutic target that could ameliorate the clinical symptoms of OA and delay the progression of OA. The

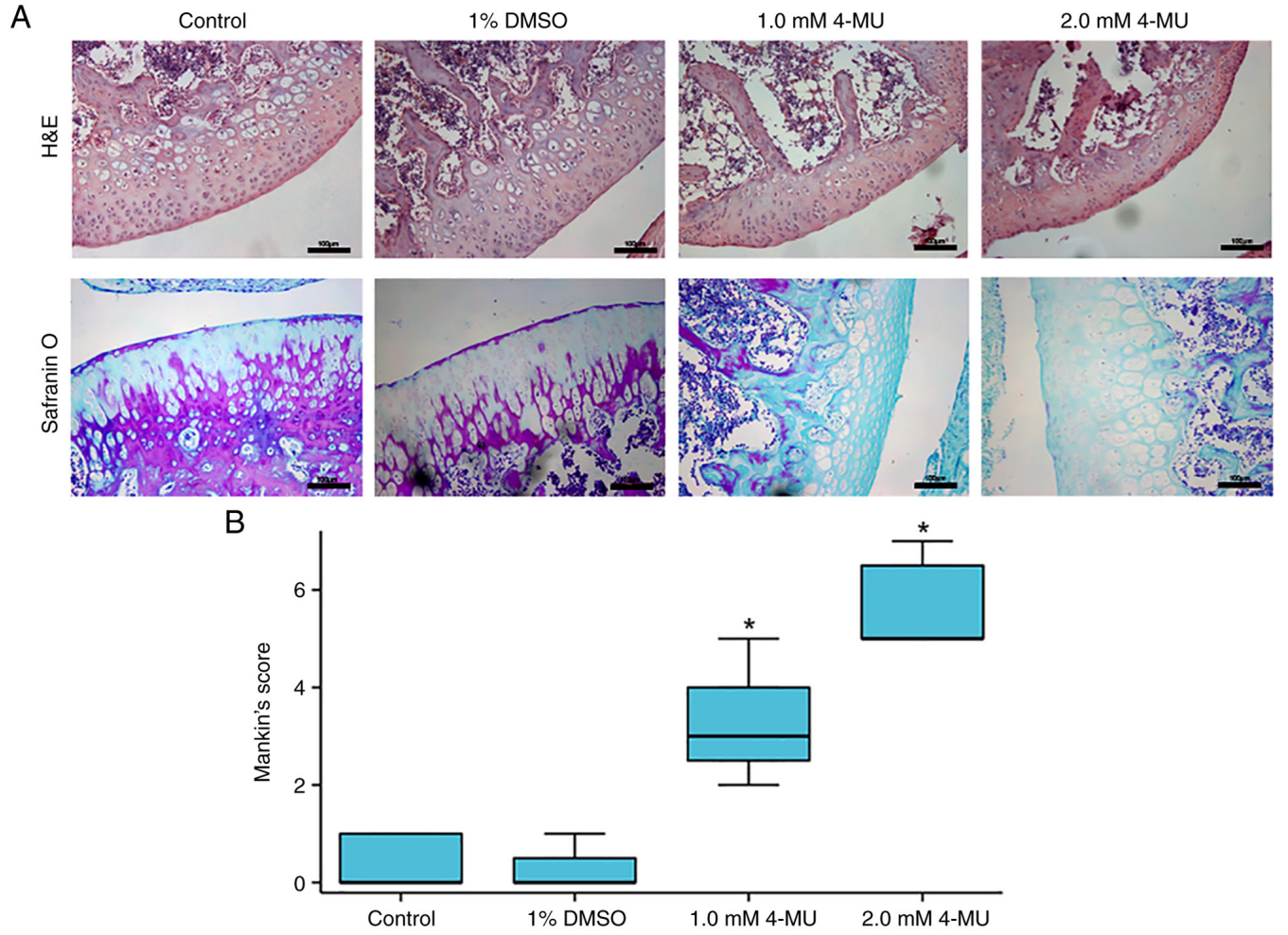

Figure 6. 4-MU inhibition of HAS-2 leads to cartilage degeneration *in vivo*. (A) H&E and safranin O staining were used to evaluate histomorphometric differences between the control, 1% DMSO, 1.0 and 2.0 mM 4-MU groups (scale bar, 100 μm). (B) Mankin's scores of cartilage in each group. The box plot shows the median, interquartile range and minimum/maximum range. *P<0.05 vs. control group, n=5 rats/group. 4-MU, 4-methylumbelliferone; H&E, hematoxylin and eosin.

present study reported the potential mechanism of cartilage degeneration following downregulation of HAS-2. Notably, to the best of our knowledge, the present study is the first in which HAS-2 has been reported to be involved in cartilage degeneration, which may provide a new target for follow-up research and the treatment of OA.

The present study used the C28/I2 cell line, which consists of immortalized normal human chondrocytes with good homogeneity. The proliferation curve of C28/I2 cells was generated and the logarithmic growth phase was determined by MTT assay. Moreover, the toxicity of 4-MU to C28/I2 cells was detected by MTT assay. Because 4-MU is insoluble in water, DMSO was used as a cosolvent in the present study. Therefore, it was necessary to detect whether the experimental concentration of DMSO had cytotoxic effects while using 4-MU. The results revealed that both the experimental concentration of 4-MU and the corresponding concentration of DMSO had no cytotoxic effect on chondrocytes and did not affect their proliferation. Subsequently, western blotting was performed to detect the effects of 4-MU on the expression levels of HAS-2 in chondrocytes. Because β-actin is not suitable for the study of the cytoskeleton (28), GAPDH was used as the internal reference protein (29). The results suggested that 4-MU could inhibit the expression of HAS-2 in chondrocytes in a concentration-dependent manner. A number of studies have used 4-MU to downregulate the function of HA, and to reveal or confirm the biological events that depend on HA (30,31). Therefore, 4-MU was used as an inhibitor of HAS-2 in the present study.

The present study also identified a notable change in the morphology of C28/I2 cells treated with 4-MU. Related studies have shown that 4-MU inhibits the synthesis of HA by consuming UDP-glucuronic acid and downregulating HAS-2 (15,32). As aforementioned, HAS-2-catalyzed synthesis of high molecular weight HA plays an important role in joint movement and maintaining intra-articular homeostasis. The HA receptor CD44 on the surface of chondrocytes can interact with various cytoskeleton proteins to activate various cytoskeleton-mediated cellular activities, such as adhesion, proliferation and migration (14,33). In addition, HA can reduce the levels of IL-1β in synovial fluid, and IL-1β can inhibit the expression of cytoskeleton-related genes, such as Fhl2, Vim and Tubb (34). These studies indicated that HAS-2 is closely related to the chondrocyte cytoskeleton. Previous studies have reported that HAS-2 appears to serve a key role in the production of HA, which is essential for normal cartilage matrix

organization and retention (35). Reduction in the formation of proteoglycan aggregates due to defective HA production in HAS-2-mutant growth plates is very likely to result in the decreased deposition of aggrecan in the matrix (36). 4-MU has been shown to inhibit HA production in various cell lines and tissue types *in vitro* and *in vivo* (15). Therefore, the present study did not measure the levels of HA; we hypothesize that the morphological changes of chondrocytes may be due to changes in the chondrocyte cytoskeleton caused by the inhibition of HAS-2 by 4-MU. Using immunofluorescence, the morphology of the cytoskeleton was observed under a LSCM, and the relative content of each cytoskeleton protein was calculated. The results showed that the expression of cytoskeleton proteins was decreased in a dose-dependent manner after 4-MU treatment, and the expression of vimentin and tubulin was significantly decreased. This is consistent with the changes in the chondrocyte cytoskeleton in OA (37,38). It has been reported that the cytoskeleton also plays an important role in phenotypic regulation, mechanical properties, and matrix synthesis and metabolism of chondrocytes. The cytoskeleton of articular chondrocytes in patients with OA was previously studied, and it was revealed that the intermediate fibers and microtubules of the cytoskeleton were significantly altered (37,39). Similar findings have also been reported in rat articular chondrocytes (38). However, as a compound inhibitor, the multiple effects of 4-MU on the body cannot be ruled out; therefore, the present study directly silenced HAS-2 to verify the regulatory impact of HAS-2 on the chondrocyte cytoskeleton from the pre-transcriptional level. The results revealed that HAS-2-shRNA could also lead to morphological changes and decreased expression of the cytoskeleton proteins of chondrocytes, which was similar to the findings observed in cells treated with 4-MU.

The RhoA/ROCK signaling pathway is an important pathway in the process of signal transduction (9). The RhoA protein is activated by mechanical and inflammatory stimulation, which can further activate downstream molecules, such as ROCK, mDia and PKN. As an important downstream signal molecule of RhoA protein, ROCK contains two isoforms, ROCK I and ROCK II. After phosphorylation by RhoA protein, ROCK can further mediate a series of downstream phosphorylation or dephosphorylation reactions, and can participate in regulation of the chondrocyte cytoskeleton (40-42). These previous studies have shown that the changes in the chondrocyte cytoskeleton are closely related to RhoA/ROCK signaling pathway. Therefore, we hypothesized that the downregulation of HAS-2 may activate the RhoA/ROCK signaling pathway and cause changes in the chondrocyte cytoskeleton. HAS-2-shRNA was used to transduce chondrocytes and the results of RT-qPCR and western blotting showed significant increases in RhoA, ROCK1 and ROCK2 expression at the gene and protein levels. However, RhoA acts as a GTPase, and it is also important to assess the 'on/off' state of these proteins (RhoA, ROCK1/2). In follow-up studies, we aim to explore the phosphorylation status of these proteins. In addition, the present study further assessed the effect of HAS-2 on the apoptosis of C28/I2 cells. The results revealed that HAS-2-shRNA promoted the apoptosis of chondrocytes. These data supported that the downregulation of HAS-2 may activate the RhoA/ROCK signaling pathway, causing changes in the chondrocyte cytoskeleton and promoting apoptosis of chondrocytes. Previous studies have also shown that the RhoA/ROCK signaling pathway can regulate the chondrocyte cytoskeleton, lead to changes in mechanical signal transduction and biomechanical properties of chondrocytes, promote apoptosis of chondrocytes and induce cartilage degeneration (21,43,44), which is consistent with the present results.

In OA, chondrocyte senescence and cartilage degeneration are accompanied by significant changes in the cytoskeleton (7,45). It has previously been shown that the cytoskeleton network of chondrocytes in old (31-months) rabbit chondrocytes is sparse, and the content of various cytoskeleton proteins is significantly lower than that in adult (8 months) and young (2 months rabbit chondrocytes. Compared with the chondrocytes in young and adult chondrocytes, the response of chondrocytes in old cells to mechanical stimulation is different because of their viscoelastic changes, which is related to the changes in the structure and cytoskeleton composition of chondrocytes (46). Some studies have used specific inhibitors of cytoskeleton proteins to study their effects on the biomechanics of chondrocytes. The results show that microfilaments and intermediate fibers mainly provide the viscoelasticity of chondrocytes. Notably, the changes in the structure and properties of cytoskeleton proteins reflect the changes in the chondrocyte cytoskeleton during OA (47). These aforementioned studies have shown that the abnormal changes of the chondrocyte cytoskeleton are closely related to cartilage degeneration. To explore whether the change in the cytoskeleton of chondrocytes can cause cartilage degeneration and lead to OA after HAS-2 inhibition, animal experiments were carried out in the present study. The results showed that 15 days after 4-MU was injected into the knee joint of Sprague-Dawley rats, the Mankin's score of cartilage tissue was significantly increased. The score was >5 in the 2.0 mM 4-MU group, thus indicating that the degree of cartilage degeneration had reached the level of early and mid-stage OA. Immunohistochemistry of cytoskeleton proteins was also carried out on the knee cartilage tissue sections. The results revealed that the number of vimentin-positive cells in the cartilage layer was markedly decreased after 4-MU injection, and only a small number of vimentin-positive cells could be found in the superficial layer of cartilage in the 2.0 mM 4-MU group. Immunohistochemical staining of actin revealed that the number of actin-positive cells was also decreased in the 4-MU groups. However, there was no notable change in the number of tubulin-positive cells in each group. These findings may be due to the short modeling time, the slow formation of OA and the slow degeneration of cartilage (48). Notably, the morphological changes in the chondrocyte cytoskeleton may be quickly detected *in vitro* with 4-MU, but the cartilage damage is not obvious in the short term because of the complexity of regulation and compensatory mechanisms *in vivo*. However, after inhibiting HAS-2 *in vivo*, vimentin was the first damaged cytoskeleton protein, followed by actin, and tubulin changed last. Therefore, these findings suggested that the downregulation of HAS-2 can destroy the chondrocyte cytoskeleton, cause cartilage degeneration and induce OA. According to a previous study, 4-MU is expected to become an effective antitumor drug widely used in the clinic (18). Unexpectedly, if 4-MU is put into a clinical application as an antineoplastic

drug, long-term use may cause cartilage degeneration and even induce OA.

In summary, the present study demonstrated that the down-regulation of HAS-2 could activate the RhoA/ROCK pathway, cause abnormal chondrocyte morphology and decrease the expression of chondrocyte cytoskeleton proteins, leading to changes in signal transduction and the biomechanical properties of chondrocytes, promotion of chondrocyte apoptosis and thus the induction of cartilage degeneration. Unfortunately, the present study did not verify the expression of HAS-2 in patients with OA or OA model animals. In addition, this study did not perform rescue experiments by adding HA to explore whether the pathological effect after HAS-2 knockout can be reversed. These experiments will be the focus of our follow-up research. Furthermore, future research will also concentrate on elucidating the key molecular mechanisms by which HAS-2 alters the cytoskeleton of chondrocytes. In addition, the clinical application of 4-MU may cause cartilage degeneration. If the expression of intra-articular HAS-2 can be upregulated at the genetic or molecular level in the early stage of OA, this may not only delay the occurrence and development of OA, but also greatly reduce the pain and risk caused by repeated intra-articular injection of HA. The latest research shows that HAS-2 overexpression diminishes the procatabolic activity of chondrocytes by a mechanism independent of extracellular hyaluronan (49), and nanotherapy-based HAS2 delivery into the joints may increase endogenous hyaluronan production, thus providing a convenient and efficient way to promote the self-repairing mechanism for OA management (50). Therefore, research on the regulation of HAS-2 as a target may provide a novel therapeutic strategy for delaying chondrocyte degeneration, and for the early prevention and treatment of OA.

Acknowledgements

Not applicable.

Funding

The present study was supported by funds from the National Natural Sciences Foundation of China (grant no. 81560366) and the Guizhou Province Science and Technology Achievement Application and Industrialization Program (Clinical Special Project) [grant no. LC (2022) 024].

Availability of data and materials

The datasets used and/or analyzed during the current study are available from the corresponding author on reasonable request.

Authors' contributions

JLY and YZ conceived and designed the experiments. JLY, YZ and LW performed the experiments. ZJZ and QS were responsible for designing and conducting the statistical analysis of the data and providing critical feedback on the interpretation of the results. JLY and ZJZ wrote the original draft of the manuscript. JLY and QS edited and finalized the final version of the manuscript. JLY and YZ confirm the authenticity of all the raw data. All authors have read and approved the final manuscript.

Ethics approval and consent to participate

Animal ethics approval was received from the Institutional Animal Ethics Review Board of Kunming Medical University (approval no. Kmmu20220992).

Patient consent for publication

Not applicable.

Competing interests

The authors declare that they have no competing interests.

References

1. French HP, Galvin R, Horgan NF and Kenny RA: Prevalence and burden of osteoarthritis amongst older people in Ireland: Findings from The Irish LongituDinal study on ageing (TILDA). Eur J Public Health 26: 192-198, 2016.
2. Roman-Blas JA, Bizzi E, Largo R, Migliore A and Herrero-Beaumont G: An update on the up and coming therapies to treat osteoarthritis, a multifaceted disease. Expert Opin Pharmacother 17: 1745-1756, 2016.
3. Gao T, Guo W, Chen M, Huang J, Yuan Z, Zhang Y, Wang M, Li P, Peng J, Wang A, *et al*: Extracellular vesicles and autophagy in osteoarthritis. Biomed Res Int 2016: 2428915, 2016.
4. Lauer JC, Selig M, Hart ML, Kurz B and Rolauffs B: Articular chondrocyte phenotype regulation through the cytoskeleton and the signaling processes that originate from or converge on the cytoskeleton: Towards a novel understanding of the intersection between actin dynamics and chondrogenic function. Int J Mol Sci 22: 3279, 2021.
5. Kwon S and Kim KS: Qualitative analysis of contribution of intracellular skeletal changes to cellular elasticity. Cell Mol Life Sci 77: 1345-1355, 2020.
6. Trickey WR, Lee GM and Guilak F: Viscoelastic properties of chondrocytes from normal and osteoarthritic human cartilage. J Orthop Res 18: 891-898, 2000.
7. Holloway I, Kayser M, Lee DA, Bader DL, Bentley G and Knight MM: Increased presence of cells with multiple elongated processes in osteoarthritic femoral head cartilage. Osteoarthritis Cartilage 12: 17-24, 2004.
8. Blain EJ: Involvement of the cytoskeletal elements in articular cartilage homeostasis and pathology. Int J Exp Pathol 90: 1-15, 2009.
9. Burridge K and Wennerberg K: Rho and Rac take center stage. Cell 116: 167-179, 2004.
10. Vigetti D, Genasetti A, Karousou E, Viola M, Clerici M, Bartolini B, Moretto P, De Luca G, Hascall VC and Passi A: Modulation of hyaluronan synthase activity in cellular membrane fractions. J Biol Chem 284: 30684-30694, 2009.
11. Recklies AD, White C, Melching L and Roughley PJ: Differential regulation and expression of hyaluronan synthases in human articular chondrocytes, synovial cells and osteosarcoma cells. Biochem J 354: 17-24, 2001.
12. Hiscock DR, Caterson B and Flannery CR: Expression of hyaluronan synthases in articular cartilage. Osteoarthritis Cartilage 8: 120-126, 2000.
13. Queisser KA, Mellema RA and Petrey AC: Hyaluronan and its receptors as regulatory molecules of the endothelial interface. J Histochem Cytochem 69: 25-34, 2021.
14. Knudson W, Ishizuka S, Terabe K, Askew EB and Knudson CB: The pericellular hyaluronan of articular chondrocytes. Matrix Biol 78-79: 32-46, 2019.
15. Kultti A, Pasonen-Seppänen S, Jauhiainen M, Rilla KJ, Kärnä R, Pyöriä E, Tammi RH and Tammi MI: 4-Methylumbelliferone inhibits hyaluronan synthesis by depletion of cellular UDP-glucuronic acid and downregulation of hyaluronan synthase 2 and 3. Exp Cell Res 315: 1914-1923, 2009.

16. Nagy N, Kuipers HF, Frymoyer AR, Ishak HD, Bollyky JB, Wight TN and Bollyky PL: 4-methylumbelliferone treatment and hyaluronan inhibition as a therapeutic strategy in inflammation, autoimmunity, and cancer. Front Immunol 6: 123, 2015.
17. Kudo D, Suto A and Hakamada K: The development of a novel therapeutic strategy to target hyaluronan in the extracellular matrix of pancreatic ductal adenocarcinoma. Int J Mol Sci 18: 600, 2017.
18. Weiz G, Molejon MI, Malvicini M, Sukowati CHC, Tiribelli C, Mazzolini G and Breccia JD: Glycosylated 4-methylumbelliferone as a targeted therapy for hepatocellular carcinoma. Liver Int 42: 444-457, 2022.
19. Livak KJ and Schmittgen TD: Analysis of relative gene expression data using real-time quantitative PCR and the 2(-Delta Delta C(T)) method. Methods 25: 402-408, 2001.
20. Afara I, Prasadam I, Crawford R, Xiao Y and Oloyede A: Non-destructive evaluation of articular cartilage defects using near-infrared (NIR) spectroscopy in osteoarthritic rat models and its direct relation to Mankin score. Osteoarthritis Cartilage 20: 1367-1373, 2012.
21. Appleton CT, Usmani SE, Mort JS and Beier F: Rho/ROCK and MEK/ERK activation by transforming growth factor-alpha induces articular cartilage degradation. Lab Invest 90: 20-30, 2010.
22. Loeser RF: Aging and osteoarthritis: The role of chondrocyte senescence and aging changes in the cartilage matrix. Osteoarthritis Cartilage 17: 971-979, 2009.
23. Poulet B and Staines KA: New developments in osteoarthritis and cartilage biology. Curr Opin Pharmacol 28: 8-13, 2016.
24. Altman RD: Practical considerations for the pharmacologic management of osteoarthritis. Am J Manag Care 15 (8 Suppl): S236-S243, 2009.
25. Varela-Eirín M, Varela-Vázquez A, Guitián-Caamaño A, Paíno CL, Mato V, Largo R, Aasen T, Tabernero A, Fonseca E, Kandouz M, *et al*: Targeting of chondrocyte plasticity via connexin43 modulation attenuates cellular senescence and fosters a pro-regenerative environment in osteoarthritis. Cell Death Dis 9: 1166, 2018.
26. Zhang M, Theleman JL, Lygrisse KA and Wang J: Epigenetic mechanisms underlying the aging of articular cartilage and osteoarthritis. Gerontology 65: 387-396, 2019.
27. DeGroot J, Verzijl N, Bank RA, Lafeber FP, Bijlsma JW and TeKoppele JM: Age-related decrease in proteoglycan synthesis of human articular chondrocytes: The role of nonenzymatic glycation. Arthritis Rheum 42: 1003-1009, 1999.
28. Leipzig ND, Eleswarapu SV and Athanasiou KA: The effects of TGF-beta1 and IGF-I on the biomechanics and cytoskeleton of single chondrocytes. Osteoarthritis Cartilage 14: 1227-1236, 2006.
29. Xu T, Yang K, You H, Chen A, Wang J, Xu K, Gong C, Shao J, Ma Z, Guo F and Qi J: Regulation of PTHrP expression by cyclic mechanical strain in postnatal growth plate chondrocytes. Bone 56: 304-311, 2013.
30. Ishizuka S, Askew EB, Ishizuka N, Knudson CB and Knudson W: 4-Methylumbelliferone diminishes catabolically activated articular chondrocytes and cartilage explants via a mechanism independent of hyaluronan inhibition. J Biol Chem 291: 12087-12104, 2016.
31. Terabe K, Ohashi Y, Tsuchiya S, Ishizuka S, Knudson CB and Knudson W: Chondroprotective effects of 4-methylumbelliferone and hyaluronan synthase-2 overexpression involve changes in chondrocyte energy metabolism. J Biol Chem 294: 17799-17817, 2019.
32. Kakizaki I, Kojima K, Takagaki K, Endo M, Kannagi R, Ito M, Maruo Y, Sato H, Yasuda T, Mita S, *et al*: A novel mechanism for the inhibition of hyaluronan biosynthesis by 4-methylumbelliferone. J Biol Chem 279: 33281-33289, 2004.
33. Bourguignon LY: Hyaluronan-mediated CD44 activation of RhoGTPase signaling and cytoskeleton function promotes tumor progression. Semin Cancer Biol 18: 251-259, 2008.
34. Joos H, Albrecht W, Laufer S, Reichel H and Brenner RE: IL-1beta regulates FHL2 and other cytoskeleton-related genes in human chondrocytes. Mol Med 14: 150-159, 2008.
35. Bastow ER, Byers S, Golub SB, Clarkin CE, Pitsillides AA and Fosang AJ: Hyaluronan synthesis and degradation in cartilage and bone. Cell Mol Life Sci 65: 395-413, 2008.
36. Matsumoto K, Li Y, Jakuba C, Sugiyama Y, Sayo T, Okuno M, Dealy CN, Toole BP, Takeda J, Yamaguchi Y and Kosher RA: Conditional inactivation of Has2 reveals a crucial role for hyaluronan in skeletal growth, patterning, chondrocyte maturation and joint formation in the developing limb. Development 136: 2825-2835, 2009.
37. Kouri JB, Jiménez SA, Quintero M and Chico A: Ultrastructural study of chondrocytes from fibrillated and non-fibrillated human osteoarthritic cartilage. Osteoarthritis Cartilage 4: 111-125, 1996.
38. Capín-Gutiérrez N, Talamás-Rohana P, González-Robles A, Lavalle-Montalvo C and Kourí JB: Cytoskeleton disruption in chondrocytes from a rat osteoarthrosic (OA)-induced model: Its potential role in OA pathogenesis. Histol Histopathol 19: 1125-1132, 2004.
39. Lambrecht S, Verbruggen G, Verdonk PCM, Elewaut D and Deforce D: Differential proteome analysis of normal and osteoarthritic chondrocytes reveals distortion of vimentin network in osteoarthritis. Osteoarthritis Cartilage 16: 163-173, 2008.
40. Strzelecka-Kiliszek A, Mebarek S, Roszkowska M, Buchet R, Magne D and Pikula S: Functions of Rho family of small GTPases and Rho-associated coiled-coil kinases in bone cells during differentiation and mineralization. Biochim Biophys Acta Gen Subj 1861: 1009-1023, 2017.
41. Langelier E, Suetterlin R, Hoemann CD, Aebi U and Buschmann MD: The chondrocyte cytoskeleton in mature articular cartilage: Structure and distribution of actin, tubulin, and vimentin filaments. J Histochem Cytochem 48: 1307-1320, 2000.
42. Ohashi K, Fujiwara S and Mizuno K: Roles of the cytoskeleton, cell adhesion and rho signalling in mechanosensing and mechanotransduction. J Biochem 161: 245-254, 2017.
43. Yang K, Wu Y, Cheng P, Zhang J, Yang C, Pi B, Ye Y, You H, Chen A, Xu T, *et al*: YAP and ERK mediated mechanical strain-induced cell cycle progression through RhoA and cytoskeletal dynamics in rat growth plate chondrocytes. J Orthop Res 34: 1121-1129, 2016.
44. Wang L, Chen G, Xiao G, Han L, Wang Q and Hu T: Cylindrospermopsin induces abnormal vascular development through impairing cytoskeleton and promoting vascular endothelial cell apoptosis by the Rho/ROCK signaling pathway. Environ Res 183: 109236, 2020.
45. Chen C, Xie J, Rajappa R, Deng L, Fredberg J and Yang L: Interleukin-1β and tumor necrosis factor-α increase stiffness and impair contractile function of articular chondrocytes. Acta Biochim Biophys Sin (Shanghai) 47: 121-129, 2015.
46. Duan W, Wei L, Zhang J, Hao Y, Li C, Li H, Li Q, Zhang Q, Chen W and Wei X: Alteration of viscoelastic properties is associated with a change in cytoskeleton components of ageing chondrocytes from rabbit knee articular cartilage. Mol Cell Biomech 8: 253-274, 2011.
47. Trickey WR, Vail TP and Guilak F: The role of the cytoskeleton in the viscoelastic properties of human articular chondrocytes. J Orthop Res 22: 131-139, 2004.
48. Ramos YF and Meulenbelt I: The role of epigenetics in osteoarthritis: Current perspective. Curr Opin Rheumatol 29: 119-129, 2017.
49. Ishizuka S, Tsuchiya S, Ohashi Y, Terabe K, Askew EB, Ishizuka N, Knudson CB and Knudson W: Hyaluronan synthase 2 (HAS2) overexpression diminishes the procatabolic activity of chondrocytes by a mechanism independent of extracellular hyaluronan. J Biol Chem 294: 13562-13579, 2019.
50. Li H, Guo H, Lei C, Liu L, Xu L, Feng Y, Ke J, Fang W, Song H, Xu C, *et al*: Nanotherapy in joints: Increasing endogenous hyaluronan production by delivering hyaluronan synthase 2. Adv Mater 31: e1904535, 2019.